Archives of Hydro-Engineering and Environmental Mechanics
Vol. 57 (2010), No. 1, pp. 31–41

Improved HLL Scheme for 1D Dam-Break Flows over Complex Topography

Xinya Ying, Sam S. Y. Wang

National Center for Computational Hydroscience and Engineering, The University of Mississippi, MS38677, USA, e-mail: ying@ncche.olemiss.edu

(Received October 07, 2009; revised February 08, 2010)

Abstract

It has been discovered that the shallow water model based on approximate Riemann solvers can produce unrealistic flows in the case of uneven topography and inaccurate solutions of discharge near hydraulic jumps. To overcome these deficiencies, we proposed a new approach to implement the HLL Riemann solver for open channel flows, including: (1) adopting a form of Saint Venant equations which have only one source term representing driving forces; (2) defining discharge at interface and evaluating it according to the flux obtained by the HLL Riemann solver. In this paper, the performance of this new method is evaluated by means of dam-break flows over a channel with triangular cross-section and a natural river valley with complex topography, respectively. Comparisons of computed results with analytic solutions and data measured from the physical model show that the proposed method is capable of satisfactorily reproducing dam-break flows over complex topography.

Key words: dam-break flow, HLL approximate Riemann solver, finite volume method, Saint Venant equations

1. Introduction

The applications of TVD schemes and approximate Riemann solvers to one--dimensional (1D) open channel flows have been frequently reported in recent times (e.g. Toro 2001, Zoppou and Roberts 2003). These schemes were originally developed to deal with gas dynamics problems. They are accurate in some situations, but problems such as unphysical flows caused by numerical imbalance and inaccuracy in the solution of discharge arise when the channel has complex geometry and the flow includes a hydraulic jump. In conventional formulation, the momentum equation includes three terms which respectively represent the hydrostatic pressure force, the pressure force due to cross-sectional variations, and the gravity effect due to bed slope. The numerical imbalance is created when these terms are calculated using different methods, which leads a numerical flow even in a still water test case, as illustrated by Rogers et al (2003) through a two-dimensional simulation of

a circular water basin with uneven bathymetry. In addition, Delis (2002) evaluated Roe's Riemann solver and several TVD schemes by means of several test cases with a hydraulic jump and revealed that the solution of discharge cannot converge at the exact solution over several cells near the hydraulic jump. These limitations restrict the applications of the TVD schemes and approximate Riemann solvers to real-life open channel flows. To overcome these deficiencies, Ying and Wang (2008) proposed a new approach to implement the HLL Riemann solver for open channel flows, including: (1) adopting the form of the Saint Venant equations which include only one source term representing driving forces; (2) defining discharge at interface and evaluating it according to the flux obtained by the HLL Riemann solver. The resulting numerical scheme has been validated and tested by means of various open channel flows with rectangular cross-sections (Ying and Wang 2008). It has been demonstrated that the scheme has excellent numerical balance and mass conservation property. In this paper, the scheme is extended to natural open channel flows with irregular cross-sections. The performance of the schemes is evaluated by means of two dam-break flow problems in a channel with triangular cross-section and a natural river valley with complex geometry, respectively. The comparisons of computed results with analytic solution and data measured from the physical model show that the scheme is capable of satisfactorily reproducing dam-break flows over complex topography.

2. Governing Equations

1D unsteady flows in a natural channel with irregular cross-sections are often described by the Saint Venant equations, that is

$$\frac{\partial \mathbf{U}}{\partial t} + \frac{\partial \mathbf{F}(\mathbf{U})}{\partial x} = \mathbf{S}(\mathbf{U}), \tag{1}$$

where, **U, F(U),** and **S(U)** are, respectively, the vectors of primitive variables, fluxes, and sources, defined as follows

$$\mathbf{U} = \begin{bmatrix} A \\ Q \end{bmatrix}, \quad \mathbf{F}(\mathbf{U}) = \begin{bmatrix} Q \\ \dfrac{Q^2}{A} \end{bmatrix}, \quad \mathbf{S}(\mathbf{U}) = \begin{bmatrix} 0 \\ -gA\dfrac{\partial Z}{\partial x} - g\dfrac{n^2 Q|Q|}{R^{4/3}A} \end{bmatrix}.$$

In above equations:

- A – cross-sectional area,
- Q – discharge,
- g – gravitational acceleration,
- Z – water surface level,
- n – Manning's coefficient,
- R – hydraulic radius (= A/P),
- P – wetted perimeter of the channel.

3. Numerical Scheme

The finite volume method is employed for solving the governing equations. Fig. 1 shows the computational grid, which has N cells, $N-1$ interfaces between cells and two boundary interfaces.

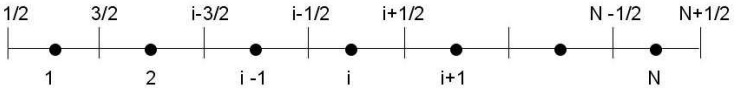

Fig. 1. Definition sketch of computational grid

Integrating Eq. (1) over the i^{th} cell with length of Δx_i yields

$$\frac{\partial}{\partial t}\int_{\Delta x_i} \mathbf{U}dx + \int_{\Delta x_i} \frac{\partial \mathbf{F}(\mathbf{U})}{\partial x}dx = \int_{\Delta x_i} \mathbf{S}(\mathbf{U})dx. \tag{2}$$

Applying Green's theorem to Eq. (2) and using an explicit scheme for time advancing, the following discretized equation is obtained,

$$\mathbf{U}_i^{n+1} = \mathbf{U}_i^n - \frac{\Delta t}{\Delta x_i}\left(\mathbf{F}_{i+\frac{1}{2}} - \mathbf{F}_{i-\frac{1}{2}}\right) + \Delta t \mathbf{S}_i, \tag{3}$$

where $\mathbf{U}_i$ is the vector of primitive variables at i^{th} cell center, representing the average values over the entire cell; $\mathbf{F}_{i+1/2}$ and $\mathbf{F}_{i-1/2}$ are the fluxes at $(i+1/2)^{\text{th}}$ and $(i\text{-}1/2)^{\text{th}}$ interfaces, see Fig. 1.

The HLL approximate Riemann solver, proposed by Harten, Lax and van Leer (1983), is used to calculate the intercell flux, because of its robustness and ease to implement. The HLL scheme assumes only one constant intermediate state between the left wave and the right wave, as shown in Fig. 2. The intercell flux is defined as

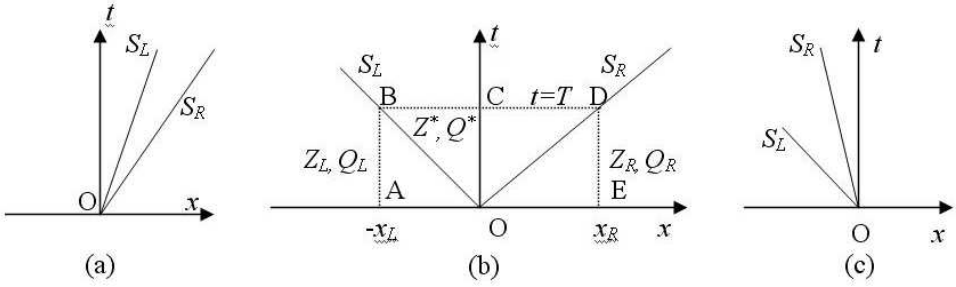

Fig. 2. Three possible wave configurations

$$\mathbf{F}_{HLL} = \begin{cases} \mathbf{F}_L \text{ when } S_L \geq 0 \\ \mathbf{F}^* \text{ when } S_L < 0 < S_R \\ \mathbf{F}_R \text{ when } S_R \leq 0, \end{cases} \tag{4}$$

where S_L and S_R are left and right wave speeds, respectively, see Fig. 2. That is, the flux at an interface is determined by the left state if $S_L \geq 0$ (Fig. 2a), and by the right state if $S_R \leq 0$ (Fig. 2c). When $S_L \geq 0$ and $S_R > 0$ (Fig. 2b), the Harten-Lax-van Leer approach provides the approximate expression for estimating $\mathbf{F}^*$. In the case of channels with irregular cross-sections, it can be written as (Ying and Wang 2008)

$$f_1^* = \frac{S_R B_R f_1^L - S_L B_L f_1^R + S_L B_L S_R B_R (Z_R - Z_L)}{S_R B_R - S_L B_L}, \tag{5}$$

$$f_2^* = \frac{S_R f_2^L - S_L f_2^R + S_L S_R (Q_R - Q_L)}{S_R - S_L},$$

where f_1^* and f_2^* are two components of the flux $\mathbf{F}^*$; B is the width of channel at water surface elevation. The wave speeds S_L and S_R are estimated according to the following equations:

$$S_L = \min\left(V_L - \sqrt{g\bar{h}_L}, V^* - \sqrt{g\bar{h}^*}\right), \tag{6}$$

$$S_R = \max\left(V_R + \sqrt{g\bar{h}_R}, V^* + \sqrt{g\bar{h}^*}\right), \tag{7}$$

where V_L and V_R are velocities of the left and right states, respectively; $\bar{h}_L$ and $\bar{h}_R$ are averaged water depth of the left and right states, which is defined according to $\bar{h} = A/B$.

$$V^* = \frac{1}{2}(V_L + V_R) + \sqrt{g\bar{h}_L} - \sqrt{g\bar{h}_R}, \tag{8}$$

$$\sqrt{gh^*} = \frac{1}{2}\left(\sqrt{g\bar{h}_L} + \sqrt{g\bar{h}_R}\right) + \frac{1}{4}(V_L - V_R). \tag{9}$$

Note that for a dry bed problem the wave speeds S_L and S_R are estimated according to the following expressions:

$$S_L = V_L - \sqrt{g\bar{h}_L}, \quad S_R = V_L + 2\sqrt{g\bar{h}_L} \text{ for right dry bed,} \tag{10}$$

$$S_L = V_R - 2\sqrt{g\bar{h}_R}, \quad S_R = V_R + \sqrt{g\bar{h}_R} \text{ for left dry bed.} \tag{11}$$

The HLL approximate Riemann solver discussed above is a 1st-order scheme. The 2nd-order spatial accuracy can be obtained through a piecewise linear reconstruction of primitive variables in each cell, which leads to

$$\mathbf{U}^{L}_{i+\frac{1}{2}} = \mathbf{U}_i + \frac{\Delta x_i}{2}\left(\frac{\partial \mathbf{U}}{\partial x}\right)_i, \tag{12}$$

$$\mathbf{U}^{R}_{i+\frac{1}{2}} = \mathbf{U}_{i+1} - \frac{\Delta x_{i+1}}{2}\left(\frac{\partial \mathbf{U}}{\partial x}\right)_{i+1}. \tag{13}$$

In order to avoid numerical oscillations, proper slope limiters must be used in estimating the slope $\partial\mathbf{U}/\partial x$. Here, the minmod limiter is adopted due to its robustness. Therefore, the slope in the i^{th} cell can be expressed by

$$\left(\frac{\partial \mathbf{U}}{\partial x}\right)_i = \text{minmod}\left(\frac{\mathbf{U}_i - \mathbf{U}_{i-1}}{x_i - x_{i-1}}, \frac{\mathbf{U}_{i+1} - \mathbf{U}_i}{x_{i+1} - x_i}\right). \tag{14}$$

The minmod function is defined as the argument with smaller value if all arguments have the same sign and otherwise it is zero.

The source terms in Eq. (3) include the water surface gradient term and the friction term. The simplest and most commonly used approach for estimating the water surface gradient is the centered difference scheme, that is,

$$\left(\frac{\partial Z}{\partial x}\right)_i = \frac{Z_{i+1} - Z_{i-1}}{x_{i+1} - x_{i-1}}. \tag{15}$$

For the 2nd-order scheme, using Eq. (15) may produce non-monotone solutions near shocks in some cases such as the idealized dam-break problem with wet bed. Therefore, we propose a new method to estimate the water surface gradient for the 2nd-order scheme, as expressed by

$$\left(\frac{\partial Z}{\partial x}\right)_i = \frac{\bar{Z}_{i+1/2} - \bar{Z}_{i-1/2}}{\Delta x_i}, \tag{16}$$

where $\bar{Z}_{i+1/2} = \left(Z^{L}_{i+1/2} + Z^{R}_{i+1/2}\right)\Big/ 2$ and $\bar{Z}_{i-1/2} = \left(Z^{L}_{i-1/2} + Z^{R}_{i-1/2}\right)\Big/ 2$ are respectively the average water surface levels at the right and the left interface of i^{th} cell.

The friction term is explicitly evaluated based on the pointwise method. Therefore, the values of Z and Q at next time can be obtained by solving Eq. (3) explicitly. Such a method is often referred to as the cell centered scheme as both variables Z and Q are defined at cell centers. However, the solution of the discharge from such a numerical scheme is not accurate in the event that there is a hydraulic jump, as shown in many numerical tests (e.g. Delis 2002, Ying and Wang 2008). To eliminate this problem, we choose the values of flux f_1 as the solution of discharge, while

the values of Q_i calculated by Eq. (3) are only used to define the constant states of the Riemann problems.

Like most explicit schemes, the schemes discussed above are subject to the Courant-Friedrichs-Lewy stability condition, that is

$$N_{CFL} = \max\left[\frac{\Delta t}{\Delta x_i}\left(|V_i| + \sqrt{\frac{gA_i}{B_i}}\right)\right] \leq 1 \ (1 \leq i \leq N). \tag{17}$$

4. Numerical Tests

The resulting numerical scheme has been validated and tested by means of various open channel flows with rectangular cross-sections (Ying and Wang 2008). Herein, two test examples with analytic solutions or measured data are selected to examine the performance of the proposed scheme in the case of channels with non-rectangular cross-sections. Example 1 is the dam-break problem in a channel with triangular cross-section. Example 2 is a real-life dam-break flow problem with complex topography. In both test examples, the 2nd-order scheme was used.

4.1. Idealized Dam-Break Problem in a Channel with Triangular Cross-Section

In this test example, the channel has a triangular cross-section with side slope 1:1. The channel is 2000 m long and is assumed to be horizontal and frictionless. A dam is located at 500 m from the upstream end of the channel. Initially, water depth is 10 m at the upstream side of the dam, and the downstream channel is dry. The domain is discretized into 1000 cells.

The numerical result at 30 s after the dam failure is compared with an exact solution (Henderson 1966) in Fig. 3. It is observed that both predicted water depth and discharge are in very good agreement with the exact solutions.

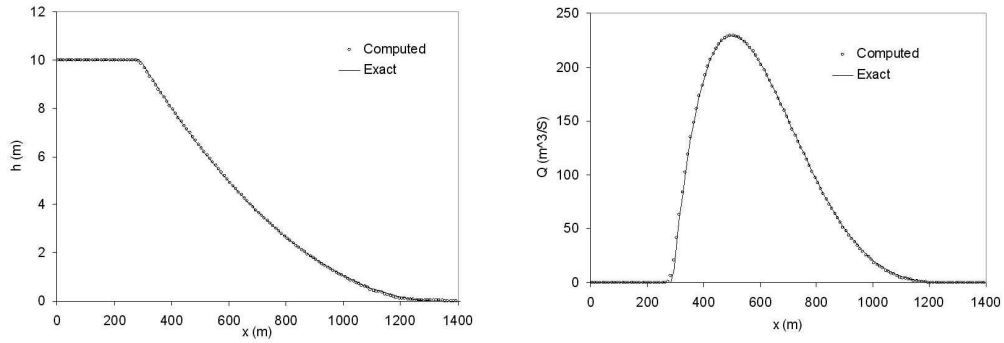

(a) water depth (b) discharge

Fig. 3. Numerical solutions of dam-break problem in an open channel with triangular cross-section at t = 30 s

4.2. Propagation of Flood Wave in the Toce River Valley

This test example, which was used as a benchmark test case in the CADAM project (Soares Frazao et al 2000), is selected to demonstrate the numerical model's capability to deal with a real-life problem with irregular cross-sections and a non-uniform grid. The topography of the Toce River is shown in Fig. 4. The computational domain was divided into 61 non-uniform cells, with lengths varied from 0.25 to 1.94 m, as shown in Fig. 5. Fig. 6 shows the discharge-time hydrograph of inflow. A free outflow boundary condition was imposed in the computation. The value of the Manning's coefficient was 0.02 s/m$^{1/3}$, as used in most of previous 1D simulations of this test case (e.g. Soares Frazao and Zech 1999, Rosu and Ahmed 1999). The entire domain was assumed to be dry at initial time. In the computation, the initial water depth in the domain was set to 0.01 m. The time step was 0.1 s and the corresponding maximum value of N_{CFL} was 0.7. The total number of time steps was 1800. The computational time was 0.33 s on a PC with AMD Athlon processor (1.46 GHz). The topographic data and inflow discharge hydrograph used in the computation were the same as those in the physical model to allow the numerical results to be directly compared with the experimental data.

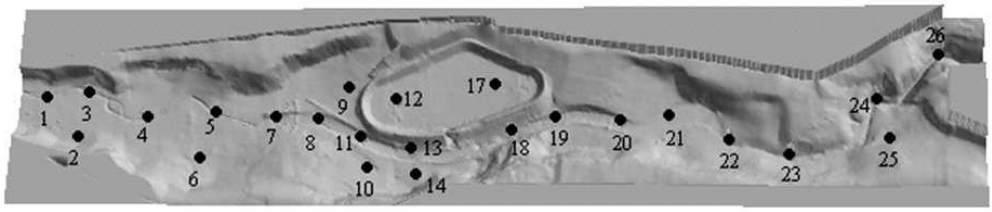

Fig. 4. Topography of Toce River Valley and locations of measurement points

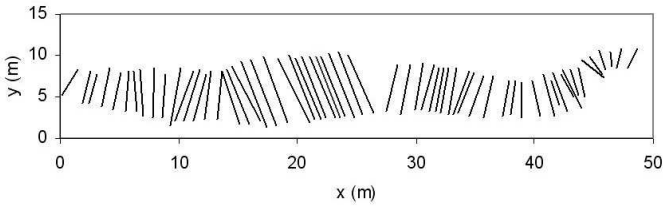

Fig. 5. Locations of computational cross-sections for Toce River test case

Computational results of water surface level and discharges at $t = 30, 60$, and 120 s are presented in Figs. 7 and 8, respectively. These figures provide a general idea about flood propagation in the river valley. In Fig. 7, a variation of water surface level, due to uneven topography and formation of hydraulic jumps, is observed. The presence of hydraulic jumps can be confirmed from Fig. 8, which displays the

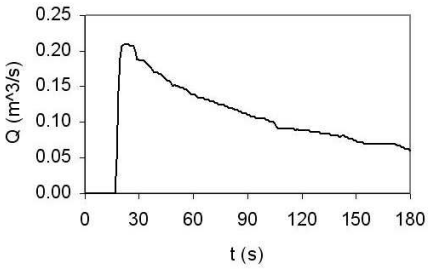

Fig. 6. Discharge-time hydrograph at inflow boundary for Toce River test case

Froude number as a function of distance x clearly revealing that there are several transitions between supercritical flow and subcritical flow. The predicted discharge as a function of distance x is presented in Fig. 9. Therein, the conventional and the newly proposed HLL schemes are referred to as HLL-A and HLL-B schemes, respectively. The former defines discharge at cell center and calculates it based on the momentum equation. The latter defines discharge at interface and evaluates it according to the flux obtained by the HLL Riemann solver. It is observed that the HLL-B scheme produces reasonable solutions, whereas the HLL-A scheme fails to correctly predict the discharges at the locations where hydraulic jumps take place. To further demonstrate the conservation property of the HLL-B scheme, a steady flow test case is performed in which a constant discharge of 0.1 m^3/s is imposed at the inlet boundary and no distinguishable difference between predicted discharge and the exact value over the entire domain is observed.

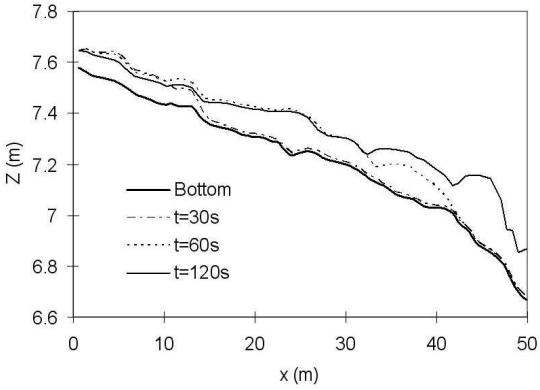

Fig. 7. Computed water surface elevations at t = 30, 60, and 120 s for Toce River test case

Fig. 10 shows that the computed stage-time hydrographs at four selected observation points are in good agreement with the measured data. Note that the numerical result represents the average value over a cross-section, while the experimental result represents the value at an observation point. This is a probable cause for the discrep-

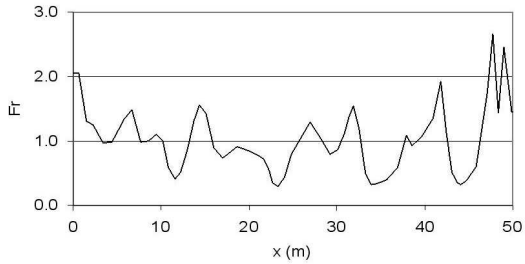

Fig. 8. Froude number Fr as a function of x at t = 120 s for Toce River test case

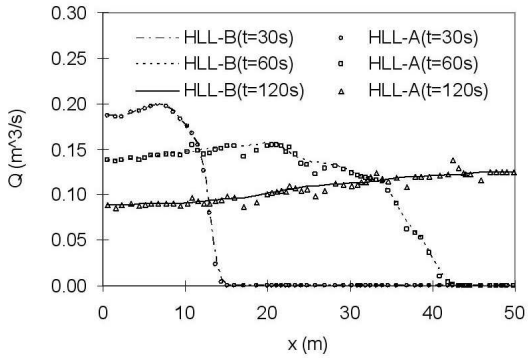

Fig. 9. Computed discharges at t = 30, 60, and 120 s for Toce River test case

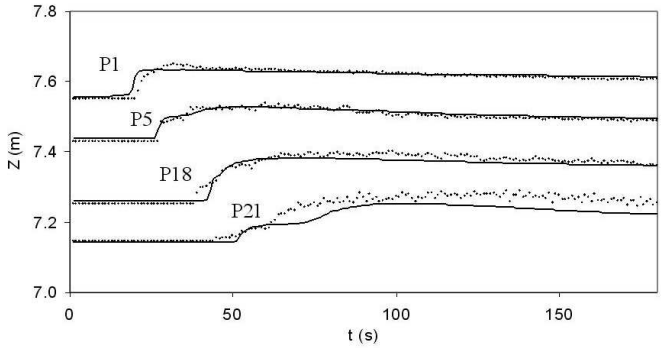

Fig. 10. Comparisons of computed stage-time hydrographs (solid line) with measured data (dot) at four observation points for Toce River test case

ancy between predicted and measured results in certain regions. Fig. 11 shows that the computed results of maximum water level are in reasonable agreement with the measured data from the physical model, except for the observation point P9 where the predicted maximum water level is lower than the measured value because the

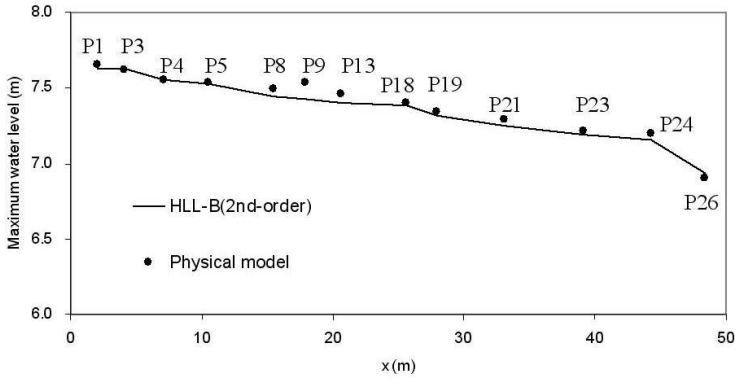

Fig. 11. Comparisons of maximum water level among numerical results and measured data for Toce River test case

local water surface rise due to the influence of reservoir embankment can not be correctly reproduced by a 1D model.

5. Conclusions

A numerical model for 1D dam-break flows has been developed based on the finite volume method. The HLL approximate Riemann solver is used to calculate intercell fluxes. To overcome numerical imbalance as well as inaccurate discharge solution near a hydraulic jump, we proposed a new approach to implement the HLL Riemann solver for open channel flows, including: (1) adopting the form of the Saint Venant equations which have only one source term representing driving forces; (2) defining discharge at interface and evaluating it according to the flux obtained by the HLL Riemann solver. The performance of this new method is evaluated by means of dam-break flows over a channel with triangular cross-section and a natural river valley with complex topography, respectively. The comparisons of computed results with analytical solutions and experimental data demonstrate that the proposed scheme is capable of correctly depicting 1D dam-break flows over complex topography that may include discontinuities and transcritical flows.

Acknowledgments

This work is a result of research sponsored by the USDA Agriculture Research Service under Specific Research Agreement No. 58-6408-2-0062 (monitored by the USDA-ARS National Sedimentation Laboratory) and the University of Mississippi.

The authors are very grateful to Dr. Sandra Soares Frazao (University Catholique de Louvain) for her help in providing the data set for the model validation in this paper.

References

Delis A. I. (2002) Higher Order Numerical Methods Evaluation for the Computation of One Dimensional Free Surface Shallow Water Flows, *Int. J. of Comput. Engrg. Science*, **3** (1), 13–55.

Harten A., Lax P. D., van Leer B. (1983) On Upstream Differencing and Godunov-type Schemes for Hyperbolic Conservation Laws, *SIAM Review*, **25** (1), 35–61.

Henderson F. M. (1966) *Open Channel Flow*, McGraw Hill Publishing, New York.

Rogers B. D., Borthwick A. G. L., Taylor P. H. (2003) Mathematical Balancing of Flux Gradient and Source Terms Prior to Using Roe's Approximate Riemann Solver, *J. Comput. Phys.*, (192), 422–451.

Rosu C., Ahmed M. (1999) Toce River Dam-Break Test Case – A Comparison Between the ISIS Numerical Model and the Physical Model, *Proc. of the 3rd CADAM workshop*, Milan, Italy.

Soares Frazao S., Morris M., Zech Y. (2000) *CADAM Project CD-ROM*, Produced by Hydraulics Division, Civil Engrg. Dept., Univ. Catholique de Louvain, Belgium.

Soares Frazao S., Zech Y. (1999) Computation of Extreme Flood Flow Through the Toce Valley, *Proc. of the 3rd CADAM workshop*, Milan, Italy.

Toro E. F. (2001) *Shock-Capturing Methods for Free-Surface Shallow Flows*, John Wiley & Sons Ltd.

Ying X., Wang S. S. Y. (2008) Improved implementation of the HLL approximate Riemann solver for one-dimensional open channel flows, *J. of Hydraul. Research*, **46** (1), 21–34.

Zoppou C., Roberts S. (2003) Explicit Schemes for Dam-Break Simulations, *J. Hydraul. Engrg,* **129** (1), 11–34.